Report on the CCPR Pilot Comparison

Spectral Responsivity 10 nm to 20 nm

reported by
Frank Scholze
Physikalisch-Technische Bundesanstalt
Berlin
Germany

October 2009

CONTENTS

Foreword

The present report concerns the pilot comparison of spectral responsivity measurements in the wavelength range 10 nm to 20 nm, piloted by PTB.

It is based on the following documents:

Recommendation of the CCPR Working Group on Key Comparisons, June 2003

Protocol of CCPR WG-UV meeting in October 2005

Technical protocol of pilot comparison of spectral responsivity measurements in the wavelength range 10 nm to 20 nm, July 19th, 2006.

1 Introduction

Under the Mutual Recognition Arrangement (MRA)[1] the metrological equivalence of national measurement standards will be determined by a set of key comparisons chosen and organized by the Consultative Committees of the CIPM, working closely with the Regional Metrology Organizations (RMOs). At the CCPR WG-UV meeting in October 2005 it was decided that a pilot comparison of spectral responsivity in the 10 nm to 20 nm range should be commenced with.

The technical protocol, covering the technical procedure to be followed during the measurement of the transfer standard detectors, was drawn up by PTB as the pilot laboratory. The procedure followed the guidelines established by the BIPM[2] and is based on current best practice in the use of standard detectors and incorporates the experience gained at PTB.

2 Participants

Participants are NIST, NMIJ, and PTB, PTB acting as the pilot laboratory.

Name	**Contact person**	**Coordinates**
NIST	Robert Vest	100 Bureau Drive, Stop 8411 Gaithersburg, MD 20899-8411 USA phone: + 1 301 975-3992 fax: + 1 301-208-6937 email: robert.vest@nist.gov
NMIJ/AIST	Terubumi Saito	1-1-1 Umezono, Tsukuba-Shi 305-8563 Ibaraki Japan phone: + 81 29 861 5654 fax: + 81 29 861 5657 email: t.saito@aist.go.jp
PTB	Frank Scholze	Abbestraße 2-12 10587 Berlin Germany phone: + 49 30 6392 5094 fax: + 49 30 6392 5082 email: frank.scholze@ptb.de

[1] MRA, Mutual Recognition Arrangement, BIPM, 1999.

[2] T.J. Quinn, "Guidelines for CIPM Key Comparisons", 1 March 1999, BIPM

3 Principle of Comparison

The comparison was carried out through the calibration of a group of transfer standard detectors. These detectors have been shown to have reasonable short-term stability and were used to transfer a spectral responsivity scale maintained in a participating laboratory to that of the pilot laboratory. Two sets of three diodes of types AXUV and SXUV from International Radiation Detectors, Inc. were used for the comparison.

The comparison had the form of a star comparison: Pilot – lab A – pilot - lab B – pilot, PTB acting as the pilot laboratory. All results were communicated directly to the pilot laboratory.

3.1 PTB experimental set-up

The calibration of the intercomparison detectors was performed at PTB at the soft X-ray radiometry beamline at BESSY II[3]. The synchrotron radiation from BESSY II is dispersed by a grazing-incidence, plane-grating monochromator. Control of high diffraction orders is achieved by the appropriate selection of the included angle of the grating[4] and by using Al, Si and Be thin-foil transmittance filters for wavelengths above 17.2 nm, between 17.2 nm and 12.4 nm, and below 12.4 nm, respectively. In the wavelength range of the pilot comparison, the monochromator was operated with a fixed included angle of 154° and an exit slit width of 1.2 mm. The resolution limit resulting from the BESSY II source size and optical aberrations[5] corresponds to only 0.2 mm exit slit width. The spectral shape of the resulting bandpass is therefore almost rectangular. A comparison of the spectral resolution at the participants' beamlines is shown in Fig. 1.

For the calibration of the set of key comparison transfer detectors, their responsivity was measured by direct comparison to the cryogenic electrical substitution radiometer (ESR) of PTB for the hard and soft X-ray spectral ranges[6], used as the primary standard detector. A set of another three detectors was also calibrated with the key comparison transfer detectors by comparison to the ESR but was kept at PTB and stored in dry air to detect any non-regularities in the key comparison measurements.

3.2 NIST experimental set-up

The calibration of the intercomparison detectors was performed at NIST on beamline 9 (BL-9)[7] of the Synchrotron Ultraviolet Radiation Facility (SURF III). The synchrotron radiation from SURF III is dispersed by a grazing-incidence, toroidal-grating monochromator[8]. The monochromator includes two

---

[3] R. Klein, C. Laubis, R. Müller, F. Scholze, G. Ulm, "The EUV metrology program of PTB", Microelectronic Engineering **83**, 707-709 (2006)

[4] F. Scholze, B. Beckhoff, G. Brandt, R. Fliegauf, R. Klein, B. Meyer, D. Rost, D. Schmitz, M. Veldkamp, "The new PTB-beamlines for high-accuracy EUV reflectometry at BESSY II", Proc. SPIE **4146**, 72 – 82 (2000)

[5] F. Scholze, J. Tümmler, G. Ulm, "High-accuracy radiometry in the EUV range at the PTB soft x-ray beamline", Metrologia **40**, S224 - S228 (2003)

[6] H. Rabus, V. Persch, and G. Ulm, "Synchrotron-Radiation Operated Cryogenic Electrical-Substitution Radiometer as High-Accuracy Primary Detector Standard in the Ultraviolet, Vacuum Ultraviolet and Soft X-ray Spectral Ranges", Appl. Opt. **36**, 5421-5440 (1997)

[7] R. E. Vest, Y. Barad, et al., "NIST VUV Metrology Programs to Support Space-Based Research," Advances in Space Research **37**, 283-296 (2006), and
R. E. Vest, L. R. Canfield, et al., "NIST programs for radiometry in the far ultraviolet spectral region," Proc. SPIE **3818**, 15-26 (1999)

[8] L.R. Canfield, "New far UV detector calibration facility at the National Bureau of Standards", Appl. Opt. **26**, 3831-3837 (1987)

gratings with identical figure specifications but a factor of four difference in ruling density: 300 mm^{-1} for long wavelengths and 1200 mm^{-1} for short wavelengths. A 1 mm fixed exit slit selects a narrow band of radiation around the tuned wavelength. The resolution at 1 mm exit slit width is shown in Fig. 1. The intercomparison range of 10 nm to 20 nm spans the transition from the short-wavelength grating to the long-wavelength grating; both were used for the intercomparison measurements, with at least two wavelengths of overlap. Control of high diffraction orders is achieved by appropriate selection of the stored-electron energy in SURF III and a 250 nm thick Be filter in BL-9.

Each intercomparison sample was compared by a direct substitution method with a working standard photodiode, the responsivity of which is known. The sample responsivity is determined from the measured ratio of photocurrents and the known responsivity of the working standard detector. Working standard detector calibrations were performed on beamline 7 (BL-7)[9] at SURF III. The optical power available at BL-9 does not provide an optimum signal-to-noise ratio in the cryogenic radiometer, and the physical space is incompatible with the operation of the cryogenic radiometer. Using the ESR as primary standard detector for measurements on BL-7, resolves both of these issues[10]. For all sample detectors, the working standard was of the same type (AXUV-100G or SXUV-100) as the sample.

The spot in BL-9 is 2.7 mm high by 3 mm wide. Both values are the full-width-at-half-maximum (FWHM). The vertical distribution is a top-hat profile. That is, there is a plateau across the beam with a steep drop at the top and bottom edges. The vertical direction is the dispersion direction of the monochromator, and the edges are defined by the exit slit edges. The horizontal distribution is a Gaussian profile. The horizontal size varies somewhat with beam current but was maintained near 3 mm in width for all intercomparison measurements.

3.3 NMIJ experimental set-up

3.3.1 Measurement facility

NMIJ spectral responsivity calibration beamline 3-1 of TERAS[11] was used for the measurements. The beamline mainly consists of a pre-focusing toroidal mirror, a filter selector, a toroidal grating monochromator, ionization chamber and an alignment stage for the detector under test (DUT). The monochromator exit slit coincides with the entrance aperture of the ionization chamber. An aperture stop of 3 mm in diameter is used in front of the DUT to clearly define the beam size for the comparison of different detectors. Further details of the monochromator are given in Table 1.

As a primary standard detector, a rare gas ionization chamber is used, specially designed with four stacked ion collectors and an off-centre cylindrical electron collector[12,13]. The periodic length of the ion collecting stage is 62 mm. The axis of the ion collectors and the axis of the electron collector lie 40 mm and 17.5 mm apart from the optical axis. Neon gas was used in the wavelength range from 10 nm to 45 nm.

---

[9] C. Tarrio, S. Grantham, and T. Lucatorto, “Facility for extreme ultraviolet reflectometry of lithography optics”, Metrologia **40**, S229–S232 (2003)

[10] C. Tarrio, S. Grantham, et al., "A simple transfer-optics system for an extreme-ultraviolet synchrotron beamline", Rev. Sci. Instrum. **76**, 046105 (2005)

[11] T. Saito and H. Onuki, "Design and performance of a beamline for VUV detector calibration", J. Spectroscopical Soc. Jpn. **43**, 385-393 (1992)

[12] T. Saito and H. Onuki, "Detector calibration in the 10-60 nm spectral range at the Electrotechnical Laboratory", J. Optics **24**, 23-30 (1993)

[13] T. Saito and H. Onuki, "Detector calibration in the wavelength region 10 nm to 100 nm based on a windowless rare gas ionization chamber", Metrologia **32**, 525-529 (1995/96)

Photon flux Φ of the incident photon beam is given by:

$$\Phi = \frac{i_2}{e\gamma a(1-a)}, \text{ with } a = \frac{i_3}{i_2}$$

and with e being the elementary charge, γ the photo ionization yield, i_2 the ion current of the second stage, and i_3 the ion current of the third stage. Si photodiodes (IRD AXUV-100G) are used as laboratory transfer standards.

3.3.2 Scale realization

The NMIJ spectral responsivity standard had been realized, principally based on a rare gas ionization chamber in the wavelength range from 10 nm to 90 nm, using synchrotron radiation from the electron storage ring TERAS[12,13].

The spectral quantum efficiency η of a DUT is:

$$\eta = \frac{i}{e\Phi} = \gamma a(1-a)\frac{i}{i_2},$$

with i being the photocurrent of the DUT. Since all the current measurements appear in the form of ratios, traceability to the current unit is not required.

To reduce the uncertainty due to secondary ionization and multiple ionization, the scale was amended in the wavelength range below 40 nm by using a windowless thermopile detector (Dexter 3M) as a non-selective detector. The scale was re-established by fitting the relative scale for the thermopile against the absolute scale of the ionization chamber in the wavelength range above 40 nm, where secondary and multiple ionizations are very unlikely to occur.

3.3.3 Measuring technique

Detector calibrations were performed in the following procedures: First, a working standard detector (silicon detector) was set after the aperture stop so that the incident radiation would hit the detector centre. Detector photocurrent was measured by an electrometer (Keithley 6430). The stored electron beam current monitor was simultaneously read by a multimeter. The wavelength scanning measurements were performed automatically. Second, the NMIJ working standard detector was replaced by the DUT measured in the same manner. Finally, the DUT was replaced again by the NMIJ working standard and the measurement was repeated. The number of current measurements per wavelength in a single wavelength scan was 6 for each detector (DUT and the standard). Overall, the number of the wavelength scan was 2 for each detector. An average of the 6 data of the ratio of the DUT/standard output to the monitor output for each wavelength and for each detector was used for calibration data analysis to minimize fluctuation and drift.

Measurement instruments to measure relevant quantities such as voltage, current, and temperature are all JCSS (Japan Calibration Service System) traceable and valid within the defined recalibration schedules, although traceability to these quantities is not essentially required to determine the spectral responsivity.

3.4 Comparison of measurement conditions

The main parameters of the monochromators used and the measurement conditions at each participating laboratory are summarized in Table 1. The spectral bandpass is also shown graphically to illustrate the wavelength dependence; Fig. 1.

			PTB	NIST	NMIJ
Monochromator	entrance / exit arm length	/m	17 / 8	2.0 / 0.9	1 / 1.168
	included angle at grating	/°	154	167	146
	grating line density	$/mm^{-1}$	1120	1200 or 300	950
	exit slit	/mm	1.2	1.0	1.0
	spectral band width	/nm	0.021 to 0.026	0.075 to 0.4	0.28 to 0.33
Measurement	angle of incidence at DUT		normal	normal	normal
	beam divergence	/mrad	1	12	11
	beam spot size	$/mm^2$	2 x 2	2.7 x 3	3 x 3
	diode temperature	/°C	24 to 26	21 to 22	25 to 26
	typical radiant power	/µW	0.2	0.01	2.5
	current measurement		short circuit	short circuit	short circuit
	polarity		surface grounded	surface grounded	surface grounded

Table 1 Compilation of the measurement conditions at the participating laboratories.

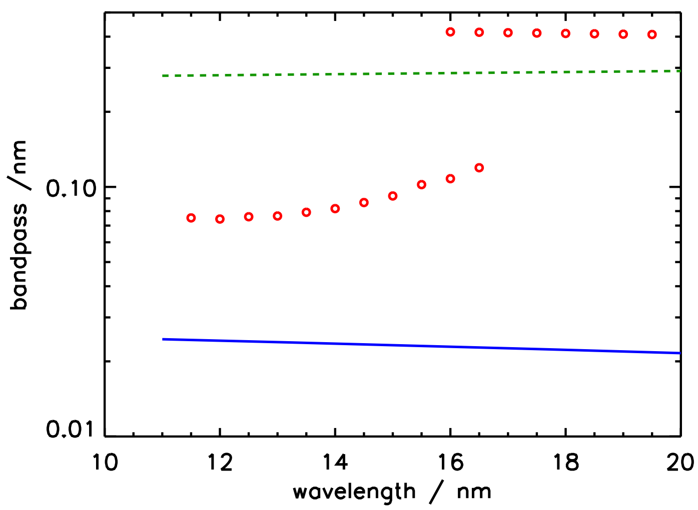

Fig. 1 Spectral bandpass used for the measurements. Values for PTB are shown by the blue line and NMIJ by the green dashes. The NIST values (circles) show a step at the wavelength where the long-wavelength grating is used.

4 Compilation of results

4.1 Uncertainty budgets of participants

4.1.1 PTB

The uncertainties for detector calibration using the ESR at PTB are published in Metrologia[5]. The numbers below are given there in Tables 3 and 4. Here, also the type of uncertainty and a statement on potential wavelength dependence are included.

Quantity	Uncertainty type	Wavelength dependence	Relative uncertainty contribution u / %
normalized heating power difference	A	indirect via radiant power	0.1
radiant energy conversion efficiency of the absorber	B	no	0.03
thermal non-equivalence between radiant and electrical heating	B	no	0.012
temperature correction for standard resistor	B	no	0.00012
calibration of standard resistor	B	no	0.001
calibration of voltmeters	B	no	0.002
Normalized radiant power			**0.11**

Table 2 Compilation of the uncertainty contributions for the measurement of a radiant power of about 0.2 µW (at 13 nm) by the cryogenic ESR. The dominant contribution is the statistical uncertainty in the determination of the heating power difference with and without radiation.

Quantity	Uncertainty type	Wavelength dependence	Relative uncertainty contribution u / %
radiant power (see Table 2)	A (B)	indirect	0.11
measured diode photocurrent	A	no	0.1
electrometer calibration factor	B	no	0.06
wavelength uncertainty (0.002 nm)	B	yes	0.01
spectral bandwidth of monochromator (0.02 nm)	B	yes	0.005
higher diffraction orders	B	yes (slightly)	0.03
diffuse scattered light	B	yes (slightly)	0.2
angle of incidence at diode (normal +/- 5°)	B	no	0.005
Spectral responsivity			**0.26**

Table 3 Uncertainty contributions for the measurement of the spectral responsivity of a photodiode at a wavelength of 13 nm.

The calibrations within the course of the pilot comparison have all been conducted with direct reference to the ESR, thus no further uncertainty contributions have to be added. The numbers in Table 2 refer to a radiant power of 200 nW. The dominant contribution to the uncertainty is the thermal noise in the power measurement, which is type A. It corresponds to an uncertainty in the power measurement of 0.2 nW radiant power at low total heating power. For spectral regions with lower radiant power (above 15 nm), this contribution increases, resulting in an increase of the total uncertainty, see Table 4. The numbers given in Table 3 apply to spectral regions with a flat response of the detectors (particularly lines 5 and 6). This does not apply to wavelengths shorter than 12.5 nm, see Fig. 2. For PTB, the uncertainties for the calibration of SXUV detectors at 12.2 nm and 12.0 nm are increased, see Table 4. The dominating uncertainty in Table 3, diffuse scattered light, covers the influence of any diffuse spectral impurity but mainly the diffuse halo of the photon beam which is detected by the larger diode (10 mm by 10 mm) and not by the smaller ESR (open aperture 6 mm diameter). This yields a systematically higher radiant power, detected by the diode.

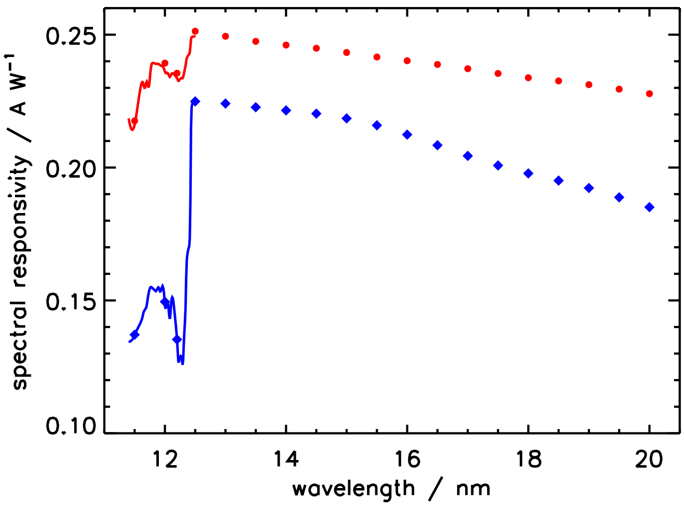

Fig. 2 Spectral responsivity of AXUV diodes (closed circles) and SXUV diodes (closed diamonds) as measured using the ESR at PTB, superimposed with high-resolution scans at the Si-L edge (solid line).

Wavelength /nm	Relative measurement uncertainty u /%	
	detector-type AXUV	detector-type SXUV
11.5	0.28	0.27
12.0	0.26	0.33
12.2	0.26	0.43
12.5	0.26	0.26
13.0	0.26	0.26
13.5	0.26	0.26
14.0	0.26	0.26
14.5	0.26	0.26
15.0	0.26	0.26
15.5	0.28	0.28
16.0	0.29	0.29
16.5	0.31	0.31
17.0	0.33	0.33
17.5	0.36	0.36
18.0	0.38	0.38
18.5	0.42	0.42
19.0	0.45	0.45
19.5	0.50	0.50
20.0	0.56	0.56

Table 4 Compilation of the PTB measurement uncertainty for the wavelengths of the comparison.

4.1.2 NIST

The NIST uncertainty budget for the spectral responsivity of the photodiodes is presented in Table 5. Generally, the relative standard uncertainty is 1% at wavelengths above 12.4 nm for all detectors.

Uncertainty Component	Uncertainty	Uncertainty in Responsivity		
			AXUV	SXUV
Radiometer electrical calibration	10 ppm		–	–
Electrical and optical power non-equivalence			< 0.10%	< 0.10%
Wavelength	0.01 nm	11.5 nm	0.80%	0.80%
		12.0 nm	0.40%	0.37%
		12.5-14.0 nm	0.01%	0.01%
		14.5-15.0 nm	0.01%	0.02%
		15.5-16.5 nm	0.01%	0.03%
		> 16.5 nm	0.01%	0.04%
Out-of-band radiation	1% of power		0.10%	0.20%
Spatially diffuse stray light		11.5 nm	1.28%	1.29%
		12.0 nm	1.05%	1.05%
		12.5-14.0 nm	0.90%	0.92%
		14.5-15.0 nm	0.90%	0.92%
		15.5-16.5 nm	0.90%	0.92%
		> 16.5 nm	0.90%	0.92%
Monochromator bandpass	0.08 nm	11.5 nm	1.60%	1.61%
		12.0 nm	0.80%	0.75%
		12.5-14.0 nm	0.02%	0.02%
		14.5-15.0 nm	0.02%	0.04%
		15.5-16.5 nm	0.02%	0.06%
		> 16.5 nm	0.02%	0.08%
Electrometer calibration			0.20%	0.20%
Statistical variance			0.30%	0.30%
Non-uniformity	0.5% (1 mm^2)		0.25%	0.25%
Total uncertainty		**11.5 nm**	**2.25%**	**2.26%**
		12.0 nm	**1.45%**	**1.43%**
		> 12.4 nm	**1.01%**	**1.04%**

Table 5 NIST uncertainty budget for intercomparison measurements.

4.1.3 NMIJ

The uncertainty contributions of NMIJ are listed in the following tables. Table 6 gives the uncertainty budget for the ionization chamber used as the primary standard detector and Table 7 compiles the further contributions for the calibration of the reference detectors. Detailed tables for the individual contributions are given in the appendix (Table 13 to Table 15).

Source of uncertainty	**Type**	**Probability distribution**	**Relative uncertainty contribution u/ %**
secondary ionization correction	B	rectangular	1.15
multiple ionization correction	B	rectangular	0.00
linearity	B	rectangular	0.87
temperature dependence（1 K）	B	rectangular	0.00
band-width dependence (0.3 nm)	B	rectangular	0.17
impurity radiation	B	rectangular	1.44
repeatability and reproducibility	A	normal	0.80
scatter and diffraction	B	rectangular	1.15
transfer to silicon photodiode	B	normal	1.91
Combined standard uncertainty			**3.34**

Table 6 Uncertainty budget for the ionization chamber and transfer to silicon detectors at 40 nm.

Source of uncertainty		Ionization chamber (Table 6)	Extra-polation (Table 13)	Calibration of standard detectors (Table 14)	Calibration of DUT AXUV (Table 14)	Calibration of DUT SXUV (Table 15)	Combined relative uncertainty AXUV	Combined relative uncertainty SXUV
Type		B	B	B	B	B		
Probability distribution		normal	normal	normal	normal	normal		
Wavelength /nm	20.0	3.34	1.49	1.27	1.27	1.34	4.1	4.1
	19.5		1.47	1.22	1.22	1.26	4.0	4.0
	19.0		1.45	1.20	1.20	1.22	4.0	4.0
	18.5		1.83	1.17	1.17	1.18	4.2	4.2
	18.0		1.45	1.09	1.09	1.10	4.0	4.0
	17.5		2.27	1.15	1.15	1.15	4.4	4.4
	17.0		2.45	0.98	0.98	0.96	4.4	4.4
	16.5		2.08	0.92	0.92	0.95	4.1	4.1
	16.0		1.54	0.87	0.87	0.90	3.9	3.9
	15.5		1.71	0.81	0.81	0.83	3.9	3.9
	15.0		1.87	0.78	0.78	0.76	4.0	4.0
	14.5		2.63	0.75	0.75	0.73	4.4	4.4
	14.0		1.80	0.73	0.73	0.72	3.9	3.9
	13.5		2.40	0.70	0.70	0.83	4.2	4.3
	13.0		2.66	0.70	0.70	1.56	4.4	4.6
	12.5		2.28	0.70	0.70	13.4	4.2	14.0
	12.2		2.53	1.11	1.11	7.42	4.5	8.6
	12.0		2.81	1.18	1.18	1.97	4.7	4.9
	11.5		2.47	1.85	1.85	2.43	4.9	5.2

Table 7 Compilation of the measurement uncertainty contributions for NMIJ (in %).

4.2 Uncertainties attributed to the transfer detectors

4.2.1 Temperature coefficient

As not all measurements are cunducted at the same operating temperature of the transfer detectors, the temperature coefficient of the responsivity has been investigated. PTB measured the temperature coefficient of both types of detectors for two representative wavelengths below and above the silicon L-absorption edge in the temperature range 25 °C to 40 °C at the wavelengths 13.5 nm and 11.5 nm, see Fig. 4 and Fig. 5, respectively. The values obtained are $3.1(1)\cdot10^{-4}$/K at 13.5 nm and $3.0\,(1)\ 10^{-4}$/K at 11.5 nm for AXUV detectors, and $3.9(2)\cdot10^{-4}$/K at 13.5 nm and $6.9\ (2)\ 10^{-4}$/K at 11.5 nm for SXUV detectors. The uncertainties are for the coverage factor k=2. These values are much closer to each other than values reported recently[14] for 13.9 and 9.2 nm.

The operating temperature for the measurements was close to 25 °C at PTB and NMIJ, and about 21 °C for NIST. Because of the bad thermal contact in vacuum - although the temperature sensors were placed in the diode housing, as shown in Fig. 3 - it is difficult to define the actual temperature of the diode die with low uncertainty. Therefore, for differences in temperature below 1 K, the measured responsivity was not corrected but an additional uncertainty of 0.03 % is included in the budget for the AXUV-type diodes and 0.04 % or 0.07 %, respectively, in the spectral ranges above and below 12.4 nm for the SXUV-type diodes. The measurement values of NIST were scaled to 25 °C using the temperature coefficients as given above. This results in a correction of +0.12 % for the AXUV detectors, and +0.15 % and +0.28 % for the SXUV-type diodes in the spectral ranges above and below 12.4 nm, respectively. It should be noted that this correction is still well below the total measurement uncertainties.

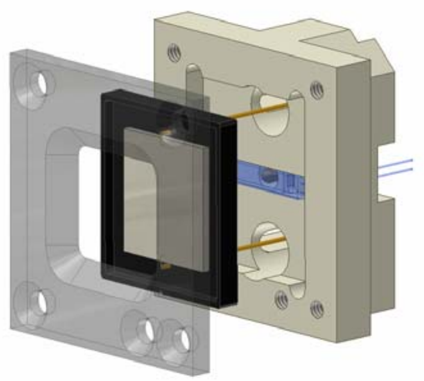

Fig. 3 Scheme of the transfer detector mount. A Pt100 temperature sensor (blue) is placed at the backside of the diode. The front side of the diode is covered by a fixed aperture, 9.5 mm by 9.5 mm in size, to avoid illumination of the outer contact area.

[14] B. Kjornrattanawanich, R. Korde, C.N. Boyer, G.E. Holland, J.F. Seely, IEEE Trans. Electr. Dev. **53**, 218 (2006)

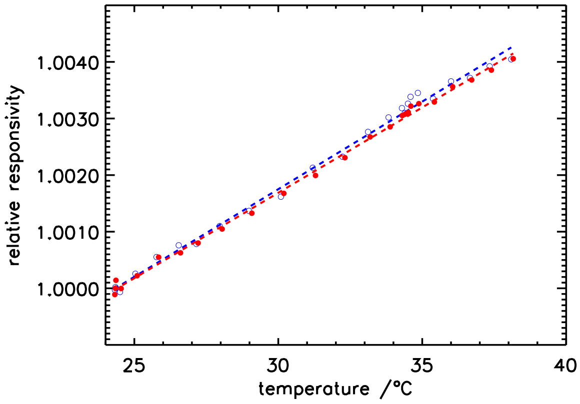

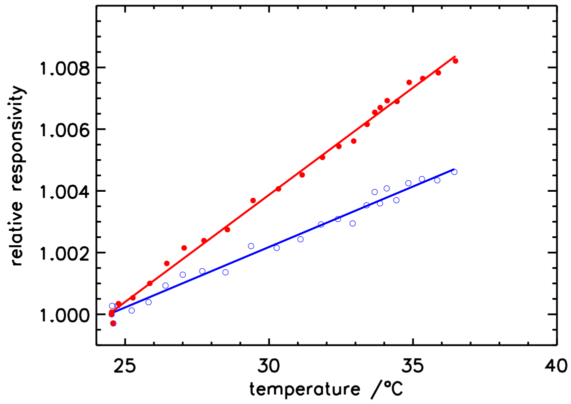

Fig. 4 Temperature dependence of the spectral responsivity for AXUV diodes measured at wavelengths of 13.5 nm (open circles) and 11.5 nm (closed circles).

Fig. 5 Temperature dependence of the spectral responsivity measured at wavelengths of 13.5 nm (open circles) and 11.5 nm (closed circles) for SXUV diodes.

4.2.2 Stability of detectors

It is known that photodiodes for the EUV spectral range can degrade[15]. On the other hand, it was necessary to have a means for detecting any issues in the reference calibrations at PTB. Therefore, PTB additionally calibrated two SXUV-type diodes (which are known to be more stable) and one AXUV each time and stored them in a dry storage cabinet. These diodes where not used for any other purpose during the time of the comparison.

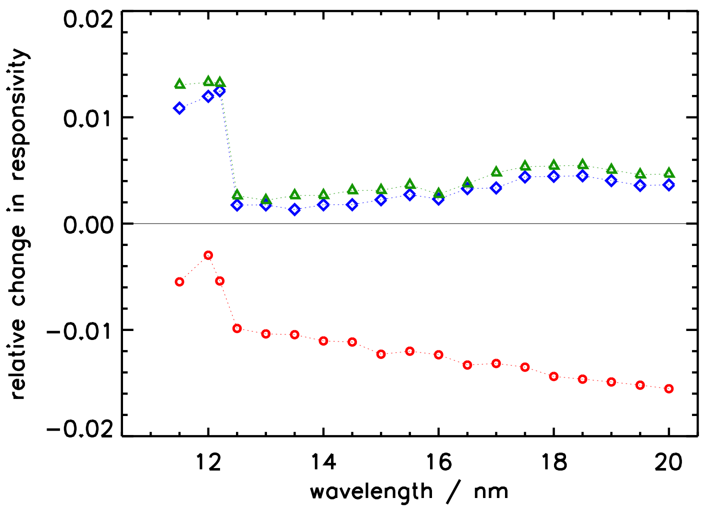

Fig. 6 Relative change of the responsivity of diodes AXUV#5 (circles), SXUV#6 (diamonds) and SXUV #13 (triangles) stored at PTB during the comparison. The responsivity measured at the end of the comparison is compared to the initially measured value.

Fig. 6 shows the relative responsivity change of diodes AXUV#5, SXUV#6 and SXUV#13 stored at PTB as measured during the comparison. For the SXUV devices a slight increase in responsivity, particularly for wavelengths shorter than 12.4 nm is obtained while the AXUV diode is degraded at all wavelengths. As the first calibration was performed directly after delivery of the diodes to PTB, the small effect at short wavelength might be explained by some initial annealing effects, yielding a slight increase in charge collection efficiency, as has been observed before for diodes of the same type[15].

[15] F. Scholze, R. Klein, T. Bock, “Irradiation Stability of Silicon Photodiodes for Extreme-Ultraviolet Radiation”, Appl. Opt. **42**, 5621-5626 (2003)

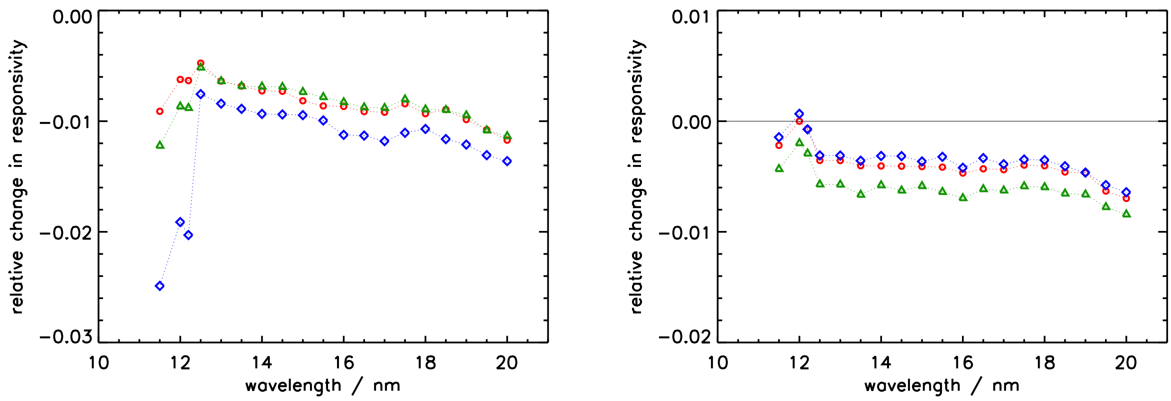

Fig. 7 Relative change in responsivity of the key comparison reference detectors: left AXUV and right SXUV detectors. Circles, diamonds and triangles represent numbers 1 to 3, respectively. The responsivity measured at the end of the comparison is compared to the initially measured value.

The responsivity of the detectors A1 to A3 and B1 to B3 used for the comparison was initially measured at PTB in week 27 of 2006, remeasured in week 09, between measurements at NIST and NMIJ, and finally in week 34 of 2007 after the diodes were returned by NMIJ. The relative change of the final value with respect to the initial calibration is shown in Fig. 7.

The intermediate measurement yielded the lowest responsivity for all but diodes A1 and A3, caused by contamination during shipment back from NIST to PTB. This particulate contamination is indicated by the spatial homogeneity maps of the diodes (Fig. 8) and is clearly seen in a microscope image as compared to a diode stored at PTB, Fig. 9. The recovery of the responsivity for the final measurements is due to the successful particle cleaning by blowing the surfaces with nitrogen gas before the measurements at NMIJ, which was carried out with consent by the pilot laboratory.

Therefore, the results from the intermediate calibration at PTB were not used for the comparison. For the NIST data, the values of the initial measurement at PTB were used for reference, and the final calibration as reference for the NMIJ data. There is good stability from the first to the last measurement, particularly for diodes B1 and B2. The AXUV-type diodes are generally somewhat worse in stability.

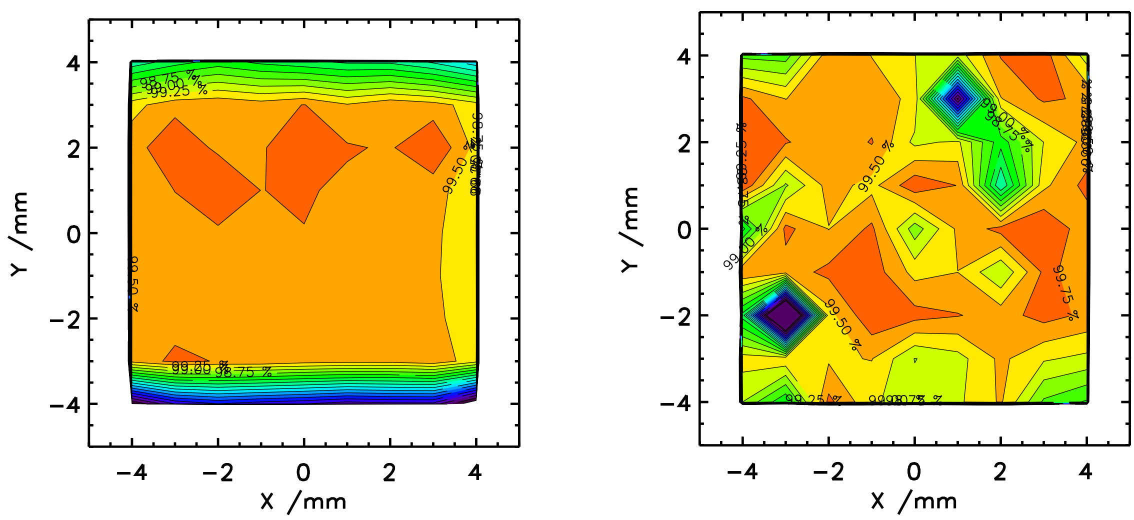

Fig. 8 Spatial homogeneity of the responsivity of diode A2 as measured initially (left) and after shipment back to PTB (right).

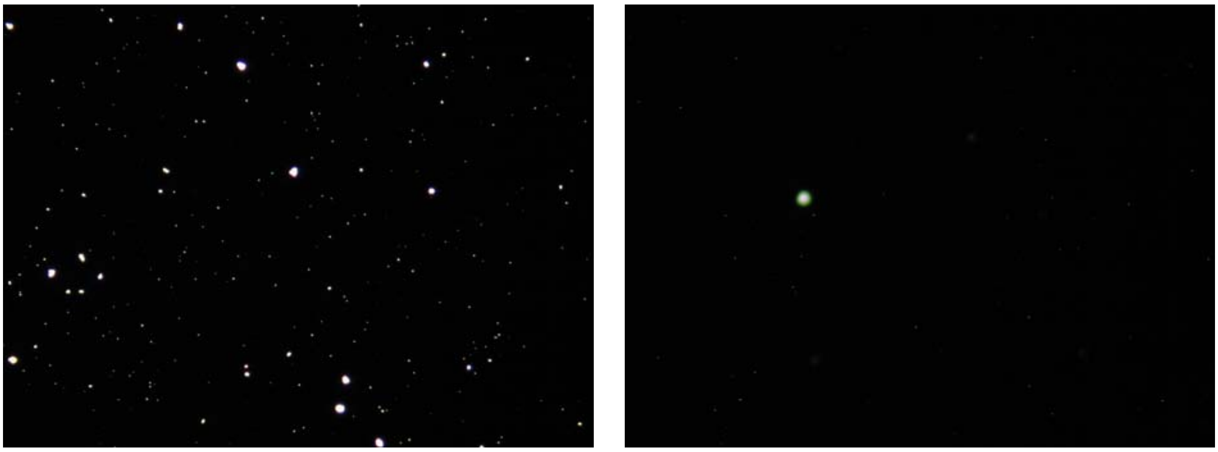

Fig. 9 Low magnification optical dark-field images of diode A2 after return from NIST (left) and diode AXUV#5 stored at PTB (right). The field shown is 1.2 mm by 1.6 mm in the centre of the diode.

The degradation of the AXUV devices is also confirmed by optical measurements of NMIJ. There, as part of the inspection of the artefacts, the spectral responsivity was also measured in the wavelength range from 200 nm to 1150 nm on arrival (April 27th, 2007) and before being shipped back to PTB (after all measurements in the EUV) on July 24th, 2007. As shown in Fig. 10, below about 400 nm a decrease in responsivity was found for detector A2. The apparent increase of 10 % above 400 nm is most probably a measurement artefact, as the spectral responsivity of A2 was about 10% lower in the whole spectral range than for the other two AXUV diodes for the first measurement. It is suspected that the electrical connection at the photodiode leads of A2 was imperfect because a connector screw of the lead was rather loose. All EUV measurements and the 2nd test measurement in the 200 nm to 1150 nm range were carried out after the screw was fastened. The other AXUV diodes show the same decrease at lower extend. At 350 nm, the absorption coefficient of Si is about 10 times higher than at 12 nm and the relative order of the responsivity changes of diodes A1 to A3 below 400 nm corresponds to the changes in the spectral range below 12.4 nm, see Fig. 7. Therefore, it is assumed that these measurements indicate damage during the EUV measurements. Note that NMIJ used the highest radiant power for the measurements, see Table 1. No notable change in the UV/VIS range was found for the SXUV photodiodes, as suspected, because of the higher irradiation stability of these diodes[15].

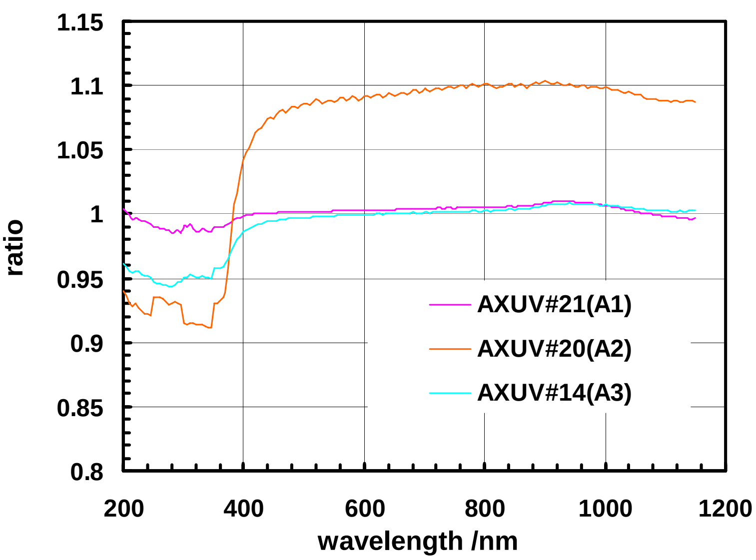

Fig. 10 Ratios of responsivity measured at NMIJ on July 24, 2007, referenced to those on April 27, 2007, for A1, A2 and A3.

Wavelength /nm	**Temperature influence /%**		**Homogeneity u /%**		**Stability u /%**		**Total uncertainty contribution u /%**	
	AXUV	**SXUV**	**AXUV**	**SXUV**	**AXUV**	**SXUV**	**AXUV**	**SXUV**
20.0	0.03	0.04	0.42	0.33	0.35	0.21	0.57	0.40
19.5	0.03	0.04	0.41	0.32	0.33	0.19	0.55	0.38
19.0	0.03	0.04	0.40	0.31	0.30	0.15	0.52	0.34
18.5	0.03	0.04	0.40	0.29	0.28	0.15	0.51	0.33
18.0	0.03	0.04	0.39	0.28	0.28	0.13	0.49	0.31
17.5	0.03	0.04	0.38	0.26	0.26	0.13	0.48	0.30
17.0	0.03	0.04	0.38	0.25	0.29	0.14	0.49	0.29
16.5	0.03	0.04	0.37	0.23	0.28	0.13	0.48	0.27
16.0	0.03	0.04	0.37	0.22	0.27	0.15	0.47	0.27
15.5	0.03	0.04	0.36	0.21	0.25	0.13	0.45	0.25
15.0	0.03	0.04	0.35	0.19	0.24	0.13	0.44	0.24
14.5	0.03	0.04	0.35	0.18	0.23	0.13	0.42	0.23
14.0	0.03	0.04	0.34	0.16	0.23	0.12	0.42	0.21
13.5	0.03	0.04	0.33	0.15	0.22	0.14	0.41	0.21
13.0	0.03	0.04	0.29	0.15	0.20	0.12	0.36	0.20
12.5	0.03	0.04	0.24	0.15	0.17	0.12	0.30	0.20
12.2	0.03	0.07	0.21	0.15	0.34	0.042	0.43	0.17
12.0	0.03	0.07	0.20	0.15	0.33	0.032	0.41	0.17
11.5	0.03	0.07	0.15	0.15	0.44	0.077	0.49	0.18
Average							**0.46**	**0.26**

Table 8 Compilation of the uncertainty contributions arising from the properties of the reference detectors used for the comparison.

The uncertainty contributions arising from the properties of the reference detectors used for the comparison are summarized in Table 8. The dominating contributions arise from the inhomogeneous responsivity of the detectors across the active surface and from the stability. The homogeneity and stability contributions differ also for the individual specimens of each type of diode. For the compilation, we took the average values for all three specimens of each type. The SXUV detectors performed better in both aspects. For the AXUV, the total contribution varies only slightly with wavelength around 0.5 %; for the SXUV detectors, homogeneity and stability improved with shorter wavelength. Here, both effects are most likely attributed to surface contamination with the transmittance of the contamination layer decreasing with increasing wavelength, as suspected for e.g. a thin organic carbon contamination. Here, the average value is 0.26 %, only about one half of the value of the AXUV diodes.

4.3 Compilation of uncertainties

The uncertainties for the measurement of the spectral responsivity stated by the participants and arising from the properties of the reference detectors are compared in Fig. 11. For NMIJ, the uncertainties for all wavelengths are higher, as compared to PTB and NIST. Primarily, this is due to the use of an ionization chamber instead of a cryogenic radiometer as the primary standard detector. For PTB and NIST, the contribution of the primary standard detector is only a minor contribution and the uncertainty budget is dominated by the contributions of the measurement with monochromatized radiation.

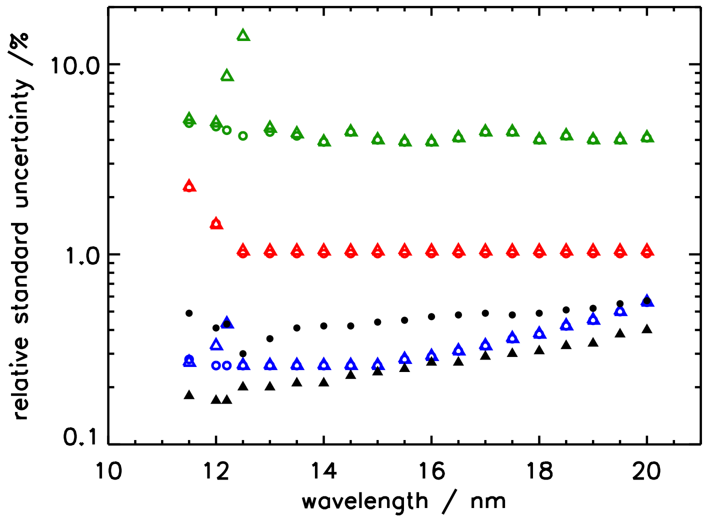

Fig. 11 Compilation of the relative standard uncertainties for the measurement of the spectral responsivity. Data are shown for AXUV (circles) and SXUV (triangles) diodes. Data of PTB, NIST, and NMIJ are shown in blue, red, and green, respectively. The solid black symbols show the uncertainty resulting from the transfer detectors, mainly due to their homogeneity and stability, see Table 8.

Also included in the compilation of Fig. 11 is the additional uncertainty from the comparison itself due to the limited homogeneity and stability of the reference detectors. Only for the SXUV detectors is this additional uncertainty lower than, although nearly equal to, the uncertainties of the calibration measurements by PTB. For future work, it is therefore desirable to have more stable and homogeneous reference detectors.

4.4 Measurement results

4.4.1 PTB

For PTB, two sets of measurements were used: The data of the initial calibration at PTB were used as reference values for the NIST measurements and the data of the final calibration, as reference for the NMIJ values; Table 9.

Wavelength /nm	Responsivity /AW^{-1}											
	A1		A2		A3		B1		B2		B3	
	initial	final	initial	final	initial	final	initial	final	initial	final	initial	final
20.0	0.2305	0.2278	0.2278	0.2247	0.2290	0.2264	0.1864	0.1851	0.1869	0.1857	0.1898	0.1882
19.5	0.2320	0.2295	0.2295	0.2265	0.2307	0.2282	0.1900	0.1888	0.1905	0.1894	0.1931	0.1916
19.0	0.2335	0.2312	0.2311	0.2283	0.2322	0.2300	0.1932	0.1923	0.1938	0.1929	0.1961	0.1948
18.5	0.2347	0.2326	0.2324	0.2297	0.2336	0.2315	0.1960	0.1951	0.1965	0.1957	0.1987	0.1974
18.0	0.2360	0.2338	0.2336	0.2311	0.2349	0.2328	0.1986	0.1978	0.1991	0.1984	0.2011	0.1999
17.5	0.2374	0.2354	0.2353	0.2327	0.2364	0.2345	0.2016	0.2008	0.2021	0.2014	0.2040	0.2028
17.0	0.2394	0.2372	0.2373	0.2345	0.2383	0.2362	0.2053	0.2044	0.2057	0.2049	0.2075	0.2062
16.5	0.2410	0.2388	0.2389	0.2362	0.2400	0.2379	0.2093	0.2084	0.2097	0.2090	0.2115	0.2102
16.0	0.2423	0.2402	0.2403	0.2376	0.2413	0.2393	0.2134	0.2124	0.2139	0.2130	0.2156	0.2141
15.5	0.2437	0.2416	0.2416	0.2392	0.2428	0.2409	0.2168	0.2159	0.2172	0.2165	0.2189	0.2175
15.0	0.2453	0.2433	0.2433	0.2410	0.2444	0.2426	0.2194	0.2185	0.2199	0.2191	0.2215	0.2202
14.5	0.2467	0.2449	0.2449	0.2426	0.2460	0.2443	0.2212	0.2203	0.2216	0.2209	0.2233	0.2219
14.0	0.2479	0.2461	0.2462	0.2439	0.2472	0.2455	0.2224	0.2215	0.2228	0.2221	0.2244	0.2231
13.5	0.2492	0.2475	0.2476	0.2454	0.2487	0.2470	0.2236	0.2227	0.2240	0.2232	0.2256	0.2241
13.0	0.2510	0.2494	0.2496	0.2475	0.2506	0.2490	0.2249	0.2241	0.2253	0.2246	0.2268	0.2255
12.5	0.2525	0.2513	0.2514	0.2495	0.2522	0.2509	0.2257	0.2249	0.2261	0.2254	0.2275	0.2262
12.2	0.2370	0.2355	0.2366	0.2318	0.2384	0.2363	0.1354	0.1353	0.1359	0.1358	0.1367	0.1363
12.0	0.2408	0.2393	0.2406	0.2360	0.2421	0.2400	0.1495	0.1495	0.1499	0.1500	0.1508	0.1505
11.5	0.2196	0.2176	0.2170	0.2116	0.2209	0.2182	0.1374	0.1371	0.1379	0.1377	0.1386	0.1380

Table 9 Responsivity measured at PTB.

4.4.2 NIST

The data received from NIST are shown in Table 10 as included in the dataset for evaluation:

Wavelength /nm	Responsivity /AW^{-1}					
	A1	**A2**	**A3**	**B1**	**B2**	**B3**
20.0	0.2340	0.2317	0.2328	0.1865	0.1870	0.1887
19.5	0.2354	0.2332	0.2344	0.1910	0.1913	0.1936
19.0	0.2367	0.2346	0.2356	0.1951	0.1955	0.1977
18.5	0.2374	0.2351	0.2359	0.1978	0.1982	0.2005
18.0	0.2382	0.2357	0.2367	0.2011	0.2015	0.2038
17.5	0.2397	0.2378	0.2387	0.2045	0.2049	0.2071
17.0	0.2425	0.2404	0.2418	0.2089	0.2094	0.2116
16.5	0.2459	0.2435	0.2445	0.2138	0.2142	0.2164
16.0	0.2457	0.2434	0.2448	0.2169	0.2173	0.2196
15.5	0.2480	0.2459	0.2475	0.2205	0.2211	0.2233
15.0	0.2493	0.2470	0.2485	0.2234	0.2238	0.2259
14.5	0.2502	0.2485	0.2497	0.2250	0.2253	0.2272
14.0	0.2517	0.2499	0.2511	0.2265	0.2267	0.2286
13.5	0.2525	0.2580	0.2521	0.2270	0.2273	0.2293
13.0	0.2539	0.2522	0.2533	0.2278	0.2282	0.2299
12.5	0.2546	0.2532	0.2541	0.2269	0.2270	0.2288
12.0	0.2447	0.2443	0.2459	0.1533	0.1535	0.1547
11.5	0.2269	0.2241	0.2290	0.1427	0.1433	0.1441

Table 10 Data of NIST received by the pilot.

4.4.3 NMIJ

The data received from NMIJ are shown in Table 11 as included in the dataset for evaluation:

Wavelength /nm	**Responsivity /AW^{-1}**					
	A1	**A2**	**A3**	**B1**	**B2**	**B3**
20.0	0.2424	0.2404	0.2405	0.1969	0.1990	0.2012
19.5	0.2437	0.2419	0.2420	0.2017	0.2034	0.2055
19.0	0.2443	0.2425	0.2426	0.2057	0.2069	0.2086
18.5	0.2456	0.2437	0.2436	0.2093	0.2104	0.2123
18.0	0.2466	0.2447	0.2445	0.2122	0.2128	0.2149
17.5	0.2474	0.2453	0.2451	0.2145	0.2148	0.2170
17.0	0.2478	0.2461	0.2462	0.2177	0.2186	0.2204
16.5	0.2485	0.2468	0.2466	0.2209	0.2211	0.2233
16.0	0.2485	0.2467	0.2466	0.2233	0.2240	0.2262
15.5	0.2493	0.2475	0.2478	0.2260	0.2268	0.2289
15.0	0.2515	0.2494	0.2499	0.2287	0.2296	0.2312
14.5	0.2530	0.2507	0.2515	0.2305	0.2312	0.2324
14.0	0.2533	0.2514	0.2518	0.2307	0.2311	0.2328
13.5	0.2545	0.2526	0.2534	0.2318	0.2325	0.2340
13.0	0.2553	0.2537	0.2545	0.2323	0.2332	0.2345
12.5	0.2502	0.2488	0.2498	0.2013	0.2045	0.2042
12.2	0.2447	0.2433	0.2428	0.1506	0.1517	0.1523
12.0	0.2445	0.2433	0.2449	0.1574	0.1585	0.1591
11.5	0.2272	0.2243	0.2271	0.1424	0.1444	0.1437

Table 11 Data of NMIJ received by the pilot.

5 Degrees of equivalence between the participants

Because of the low number of participants in the pilot comparison, no reference value is defined. The data are summarized below in terms of bilateral degrees of equivalence (DoE).

All bilateral DoE between NMIJ, NIST, and PTB are well within the k=2 confidence interval. Nevertheless, there is bias in the results, with those of NMIJ being the highest and PTB the lowest values.

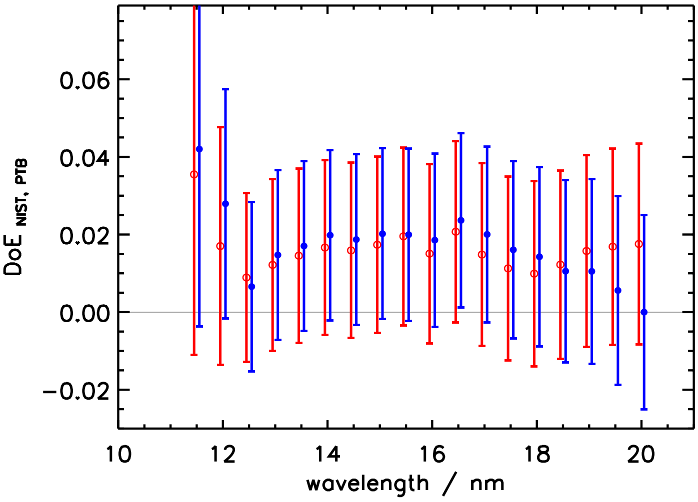

Fig. 12 DoE of NIST and PTB as function of wavelength. Red open circles are for type A diodes and blue closed circles type B diodes. The error bars are the combined uncertainty for the coverage factor k=2.

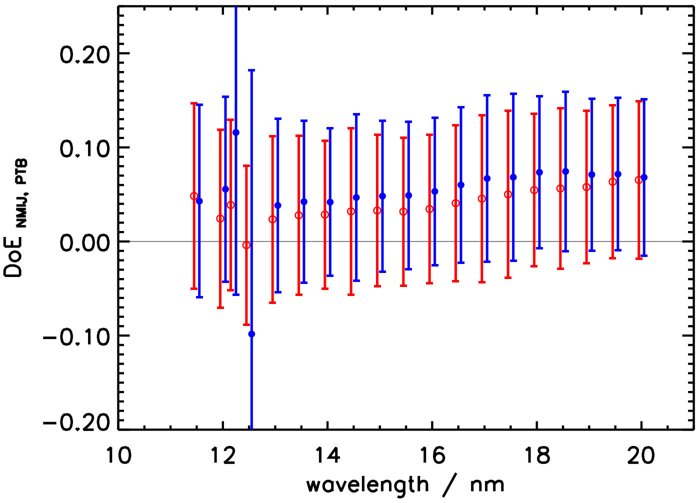

Fig. 13 DoE of NMIJ and PTB as function of wavelength. Red open circles are for type A diodes and blue closed circles type B diodes. The error bars are the combined uncertainty for the coverage factor k=2.

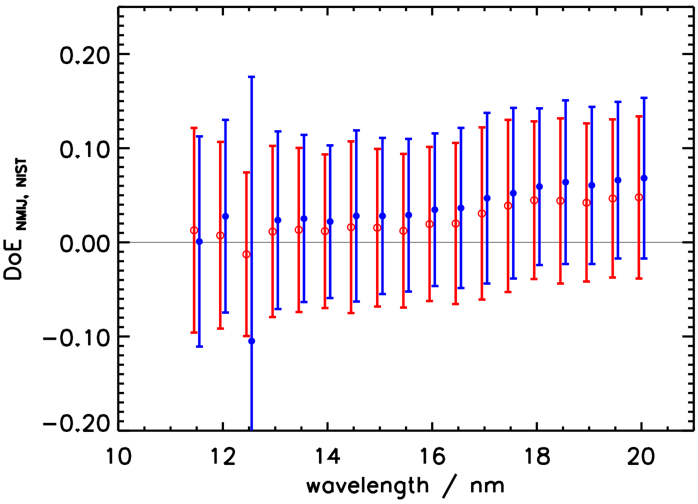

Fig. 14 DoE of NMIJ and NIST as function of wavelength. Red open circles are for type A diodes and blue closed circles type B diodes. The error bars are the combined uncertainty for the coverage factor k=2.

6 Discussion of the results

All participating laboratories in this pilot comparison used monochromatized synchrotron radiation for the measurements. PTB and NIST used a cryogenic radiometer as the primary standard detector and NMIJ an ionization chamber with extrapolation by a wavelength-independent detector. Therefore, the uncertainty budget of NMIJ contains a rather large wavelength-independent contribution for this primary detector realization which is not present in the budgets of PTB and NIST.

6.1 Analysis of uncertainty budgets

The uncertainty budgets can be separated with respect to whether the contributions depend on wavelength. The magnitude of an average offset for all wavelengths should correspond to the uncertainties not depending on wavelength, and the spread of the measured values around this offset should be covered by the wavelength-dependent contributions. Figures 15 and 16 show this kind of evaluation. The values for the DoE are shown only with the type A and the wavelength-dependent uncertainty contributions. For all institutes, the estimated uncertainties fully cover the observed variations of the measured value with respect to the average DoE within the k=2 confidence interval. The data for the average offset between the measurements are summarized in Table 12. The influence of the spatially diffuse radiation was included as a wavelength-independent uncertainty, because it changes only slightly with wavelength and always gives a systematic overestimation of the responsivity. The systematic deviations are also well within the k=2 confidence interval, indicating a consistent estimation of the measurement uncertainties of the participating laboratories.

	Uncertainty budget (wavelength independent) u* / %	DoE, average value / %	DoE / u*
NIST / PTB	1.0	1.7	1.7
NMIJ / PTB	3.5	4.6	1.3
NMIJ / NIST	3.6	2.7	0.7

Table 12 Comparison of the average value of the DoE with the wavelength-independent uncertainty contributions u*.

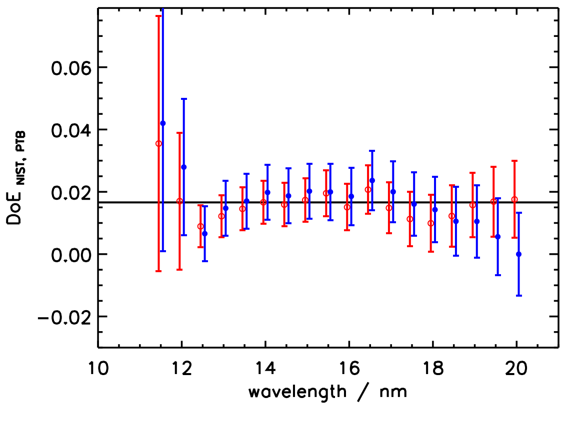

Fig. 15 DoE for NIST with respect to PTB. The average value of all detectors and all wavelengths is indicated by the horizontal line. The error bars cover only the wavelength-dependent contributions with the coverage factor k=2. Note that the diffuse stray light contribution was completely regarded as non- wavelength-dependent and removed from the partial uncertainty budget shown here.

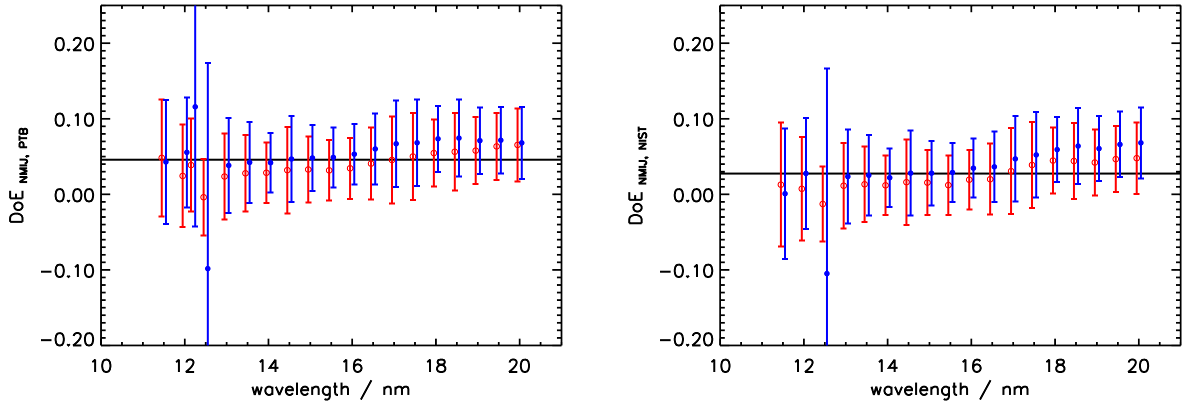

Fig. 16 DoE for NMIJ with respect to PTB (left) and NIST (right). The error bars cover only the wavelength-dependent contributions with the coverage factor k=2. The particularly high uncertainty close to the Si $L_{2,3}$ edge at 12.4 nm is due to the monochromator bandwidth, see Table 15.

6.2 Physical detector model for the reference diodes

The diffuse scattered light halo of the monochromatized photon beam always increases the apparent spectral responsivity of the detectors as measured in this pilot comparison. To check for a general offset of all measured values by all laboratories, the spectral responsivity of an AXUV-type detector was measured at the pilot laboratory down to 1 nm wavelength and a physical model was used to check the consistency of the efficiency values for the complete spectral range.

It has been shown that the responsivity of the silicon photodiodes can be understood with a constant energy of 3.66 eV per electron-hole pair and a model accounting for the absorption in the oxide front layer and some charge losses directly beneath the oxide-silicon interface[16]. Figure 17 shows the responsivity of diode AXUV#5 (stored at PTB) measured in the wavelength range from 0.827 nm (1500 eV) up to 20 nm. This measurement was performed at the end of the comparison period. According to the data shown in Fig. 6 and Fig. 7, we suspect about 1 % higher responsivity of the diodes for the first calibration. The short wavelength measurements provide us with independent information on the charge collection efficiency of this lot of AXUV diodes. For the model, the thickness of the SiO_2 top layer was set such that the relative variation around the absorption resonance at 11.5 nm is matched. The parameters for the incomplete charge collection in the model were adjusted to fit the region between 3 nm and 10 nm, where the effect is strongest. By using this approach, we also obtain a good fit of the step in responsivity at the silicon L-edge at 12.4 nm. Note that the spectral shape measured in the region above 12.4 nm is smoother than the calculation. This is due to a structure in the scattering factors of Henke et al.[17] for silicon in the range around 14 nm, which we do not observe in our measurements. Also shown in Fig. 17 is a calculation with increased charge collection efficiency such that the responsivity above 12.4 nm is increased by 2 %. Note the significantly higher difference around 10 nm. Because of this different behaviour, the shorter wavelength measurements combined with the physical model provide an independent benchmark for the responsivity in the range above 12.4 nm.

[16] F. Scholze, H. Rabus, and G. Ulm, "Mean energy required to produce an electron-hole pair in silicon for photons of energies between 50 and 1500 eV", J. Appl. Phys. **84**, 2926-2939 (1998)

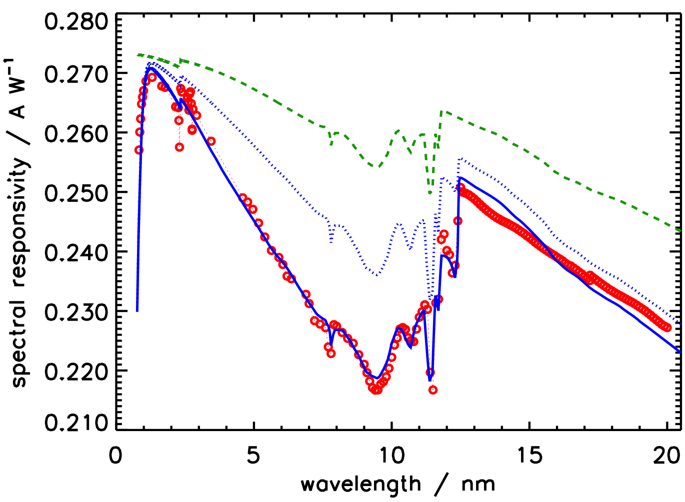

Fig. 17 Responsivity of AXUV#5, stored at PTB and measured in the wavelength range from 0.827 nm (1500 eV) up to 20 nm (open circles). The green dashed line is the transmittance of 7.5 nm SiO_2 as calculated using the scattering factors of Henke et al.[17]. The complete model calculation, including incomplete charge collection, is shown by the solid blue line. The dotted blue line shows the model with increased charge collection efficiency.

In Fig. 18 this benchmark is compared to the data measured for the AXUV diodes in the spectral range of the comparison. Here, the model-based extrapolation of the short wavelength measurements at PTB is in favour of the lower responsivity as measured at PTB.

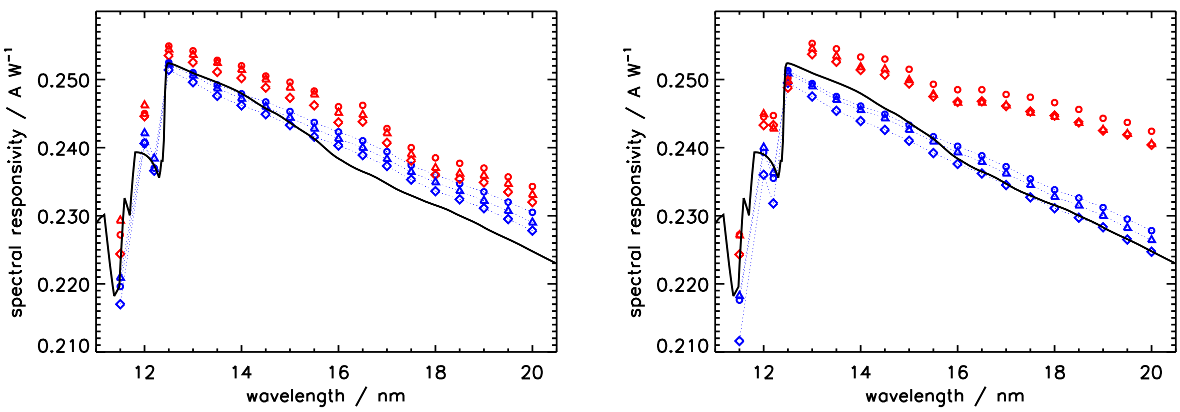

Fig. 18 Comparison of measurement results for type AXUV detectors, left: Measurements of NIST (red) and initial responsivity as measured by PTB (blue), right: values of NMIJ (red) in comparison to the final calibration results of PTB (blue). Circles, diamonds and triangles represent number 1 to 3, respectively. The solid line is the model calculation, extrapolating the responsivity measured at PTB below 10 nm. Note that the respective measurements of PTB differ by about 1 % relative (see Fig. 7). The structure around 16 nm in the calculation originates from the tabulated scattering factors[17] used for silicon.

[17] B.L. Henke, EM. Gullikson, J.C. Davis, “X-ray interactions: photoabsorption, transmission and reflection at E=50-30,000 eV, Z=1-92”, Atomic Data and Nucl Data Tables **54**, 181-342 (1993)

7 Conclusions

A comparison of spectral responsivity measurements in the 10 nm to 20 nm spectral range was performed for the first time. At this stage, only three national metrology institutes participated. All participating laboratories used monochromatized synchrotron radiation. PTB and NIST used a cryogenic radiometer as the primary standard detector and NMIJ an ionization chamber with extrapolation by a wavelength-independent detector. The primary detector realization by an ionization chamber with extrapolation results in a rather large wavelength-independent uncertainty contribution. The uncertainty contribution of the ESR as the primary standard detector is only a minor contribution in the total budget. Using an ESR, the uncertainty budgets are dominated by the contributions of the detector comparison itself using monochromatized synchrotron radiation. Among those, the dominating uncertainty is attributed to diffuse scattered light, i.e. any diffuse spectral impurity but mainly the diffuse halo of the photon beam. In the case of the standard set-up with the diode placed on a feedthrough in front of the radiometer, which usually has a smaller aperture, this yields a systematically higher radiant power detected by the diode, resulting in too high a responsivity measured.

Another significant uncertainty contribution as compared to the cryogenic radiometer is the stability and homogeneity of presently available photodiodes used as comparison reference detectors. The uncertainty attributed to the reference detectors is as large as the measurement uncertainty for the direct comparison to the cryogenic radiometer at the pilot laboratory.

All bilateral DoE are well within the respective k=2 expanded uncertainty ranges for all wavelengths. A separation of non-wavelength-dependent and wavelength-dependent uncertainty contributions is consistent with the respective mean DoE and wavelength-dependent variations of all bilateral DoE.

Future work should be focussed on the search for more stable reference detectors and a more detailed analysis of the spectral and spatial properties of the monochromatized radiation used for the calibration measurements.

8 Attachment: Detailed uncertainty contributions for NMIJ

The detailed uncertainty contributions are summarized in the following tables:

Source of uncertainty		Uniformity (position error 1.5 mm)	Linearity	Temperature dependence (1 K)	Wavelength dependence	Bandwidth dependence (0.3 nm)	Impurity radiation	Repeatability & reproducibility	Combined standard uncertainty
Type		B	B	B	B	B	B	A	
Probability distribution		rectangular	rectangular	rectangular	rectangular	rectangular	rectangular	normal	
	20.0				0.46	0.10	1.17	0.44	1.49
	19.5				0.45	0.06	1.14	0.47	1.47
	19.0				0.44	0.06	1.10	0.52	1.45
	18.5				0.43	0.06	1.01	1.30	1.83
	18.0				0.42	0.06	1.11	0.51	1.45
	17.5				0.41	0.06	0.83	1.96	2.27
	17.0				0.40	0.06	0.75	2.21	2.45
	16.5				0.39	0.06	0.64	1.82	2.08
	16.0				0.38	0.06	0.57	1.21	1.54
Wave-length /nm	15.5	0.58	0.29	0.12	0.36	0.06	0.52	1.45	1.71
	15.0				0.35	0.06	0.47	1.65	1.87
	14.5				0.34	0.06	0.41	2.49	2.63
	14.0				0.33	0.06	0.36	1.60	1.80
	13.5				0.32	0.06	0.32	2.26	2.40
	13.0				0.31	0.13	0.31	2.54	2.66
	12.5				0.30	0.12	0.30	2.14	2.28
	12.2				0.18	0.12	0.29	2.42	2.53
	12.0				0.29	0.13	0.29	2.70	2.81
	11.5				0.28	0.13	0.30	2.34	2.47

Table 13 Extrapolation (in %)

Source of uncertainty		Uniformity (position error =1.5 mm)	Linearity	Stability (1 year)	Polarization /Divergence (2 deg.)	Temperature dependence (1 K)	Wavelength uncertainty (0.06 nm)	Bandwidth dependence (0.3 nm)	Impurity radiation	Reproducibility/ repeatability	Combined standard uncertainty
Type		B	B	B	B	B	B	B	B	A	
Probability distribution		rectangular	rectangular	rectang.	normal	rectangular	rectangular	rectangular	rectangular	normal	
Wave-length /nm	40.0	0.46				0.02	0.09	0.12	1.73	0.30	1.91
	20.0	0.29				0.01	0.03	0.10	1.06	0.25	1.27
	19.5	0.28				0.01	0.03	0.06	1.00	0.27	1.22
	19.0	0.27				0.01	0.03	0.06	0.97	0.27	1.20
	18.5	0.26				0.01	0.03	0.06	0.94	0.30	1.17
	18.0	0.25				0.01	0.03	0.06	0.85	0.25	1.09
	17.5	0.24				0.01	0.02	0.06	0.93	0.26	1.15
	17.0	0.24				0.01	0.01	0.06	0.71	0.26	0.98
	16.5	0.23	0.06	0.58	0.00	0.01	0.00	0.06	0.63	0.25	0.92
	16.0	0.22				0.01	0.01	0.06	0.55	0.26	0.87
	15.5	0.21				0.01	0.03	0.06	0.50	0.16	0.81
	15.0	0.20				0.01	0.05	0.06	0.45	0.12	0.78
	14.5	0.19				0.01	0.03	0.06	0.41	0.14	0.75
	14.0	0.18				0.01	0.01	0.06	0.36	0.16	0.73
	13.5	0.17				0.01	0.00	0.06	0.32	0.14	0.70
	13.0	0.17				0.02	0.03	0.13	0.29	0.15	0.70
	12.5	0.17				0.02	0.06	0.12	0.29	0.16	0.70
	12.2	0.17				0.02	0.27	0.12	0.29	0.24	1.11
	12.0	0.17		0.98		0.02	0.49	0.13	0.29	0.24	1.18
	11.5	0.17				0.02	1.50	0.13	0.31	0.25	1.85

Table 14 Si photodiode (AXUV-100G) calibration (in %)

Source of uncertainty		**Uniformity (position error = 1.5 mm)**	**Linearity**	**Stability (1 year)**	**Polarization /Divergence (2 deg.)**	**Temperature dependence (1 K)**	**Wavelength uncertainty (0.06 nm)**	**Bandwidth dependence (0.3 nm)**	**Impurity radiation**	**Reproducibility/ repeatability**	**Combined standard uncertainty**
Type		B	B	B	B	B	B	B	B	A	
Probability distribution		rectangular	rectang.	rectang.	normal	rectangular	rectangular	rectangular	rectangular	normal	
	20.0	0.17				0.02	0.16	0.01	1.18	0.10	1.34
	19.5	0.17				0.02	0.16	0.00	1.09	0.06	1.26
	19.0	0.17				0.02	0.18	0.01	1.04	0.09	1.22
	18.5	0.16				0.02	0.17	0.00	0.99	0.16	1.18
	18.0	0.16				0.02	0.13	0.01	0.89	0.19	1.10
	17.5	0.16				0.02	0.07	0.02	0.96	0.15	1.15
	17.0	0.15				0.02	0.10	0.02	0.73	0.14	0.96
	16.5	0.15				0.02	0.25	0.01	0.63	0.27	0.95
Wave-length /nm	16.0	0.15	0.06	0.58	0.00	0.02	0.33	0.01	0.55	0.18	0.90
	15.5	0.14				0.02	0.23	0.01	0.50	0.17	0.83
	15.0	0.14				0.01	0.06	0.00	0.45	0.13	0.76
	14.5	0.14				0.01	0.08	0.00	0.40	0.12	0.73
	14.0	0.13				0.01	0.15	0.01	0.36	0.13	0.72
	13.5	0.13				0.01	0.44	0.04	0.31	0.19	0.83
	13.0	0.13				0.01	1.39	0.23	0.29	0.15	1.56
	12.5	0.13				0.01	13.34	0.23	0.32	0.04	13.36
	12.2	0.12				0.02	7.33	0.46	0.36	0.08	7.42
	12.0	0.12		0.98		0.02	1.50	0.69	0.40	0.08	1.97
	11.5	0.12				0.02	2.14	0.37	0.45	0.04	2.43

Table 15 Si photodiode (SXUV-100) calibration (in %)